Iranian Journal of Fuzzy Systems

Volume 20, Number 6, (2023), pp. 171-185

Original paper

University of Sistan and Baluchestan

Adaptive non-singular fast terminal sliding mode control and synchronization of a chaotic system via interval type-2 fuzzy inference system with proportionate controller

M. A. Labbaf Khaniki[1], M. Manthouri[2] and M. Ahmadieh Khanesar[3]

[1] *Faculty of Electrical Engineering, K.N. Toosi University of Technology, Tehran, Iran*
[2] *Electrical and Electronic Engineering Department, Shahed university, Tehran/Iran*
[3] *Faculty of Engineering, University of Nottingham, Nottingham, NG7 2RD, UK*

mohammadlabbaf@email.kntu.ac.ir, mmanthouri@shahed.ac.ir, Ezzma5@exmail.nottingham.ac.uk

Abstract

This paper introduces a novel adaptive nonsingular fast terminal sliding mode approach that benefits from an interval type-2 fuzzy logic estimator and a gain for control and synchronization of chaotic systems in the presence of uncertainty. The nonsingular fast terminal sliding mode controller is developed to increase the convergence rate and remove the singularity problem of the system. Using the proposed method, the finite-time convergence has been ensured. To eliminate the chattering phenomenon in the conventional sliding mode controller, the discontinuous sign function is estimated using an interval type-2 fuzzy inference system (FIS) based on the center of sets type reduction followed by defuzzification. By adding the proportionate gain to the interval type-2 FIS, the robustness and speed of the controller system is enhanced. An appropriate Lyapunov function is utilized to ensure the closed-loop stability of the control system. The performance of the controller is evaluated for a nonlinear time-varying second-order magnetic space-craft chaotic system with different initial conditions in the presence of uncertainty. The simulation results show the efficacy of the proposed approach for the tracking control problems. The time and frequency domain analysis of the control signal demonstrates that the chattering phenomenon is successfully diminished.

Keywords: Chaos, nonsingular terminal sliding mode control, adaptive control, interval type-2 fuzzy inference system, chattering phenomenon.

1 Introduction

Chaos theory is a fascinating phenomenon that has attracted much attention over the last four decades. Trajectories of chaotic systems are very sensitive to their initial conditions and nominal values so that two initially close trajectories may behave completely different over time. Additionally, the highly nonlinear, complex and unpredictable nature of the chaotic systems makes their analysis, stabilization, and synchronization difficult. Chaos phenomenon can be found in versatile fields such as robotic [3], computer science [21], power converters [9], networked control [37], and so on [8].

Different types of classical and intelligent control methods are proposed to control, stabilize, and synchronize the chaotic systems. In [13], a control strategy is proposed for stabilization of uncertain chaotic systems against unknown parametric and dynamic uncertainty, and disturbances by fuzzy sliding mode controller (SMC). [22] introduces the fuzzy time-delayed controller for stabilization of an unstable periodic orbit without any knowledge of the system model. [28] proposes a novel adaptive second-orders fuzzy SMC using universe fuzzy logic system to control the chaotic system. The performance of nonlinear model predictive controllers is investigated for chaotic system in [11]. [17] uses adaptive control techniques to control and synchronization of fractionalorder chaotic satellite systems. SMC as an efficient, robust and high performance controller has been received much attention to tackle nonlinearity, parameters uncertainty, and

Corresponding Author: M. Manthouri
Received: August 2021; Revised: August 2022; Accepted: February 2023.
https://doi.org/10.22111/IJFS.2023.39658.6889

external disturbance [4]. This type of controller is applied on the nonlinear systems such as chaotic systems [6], flexible robots [30], and quadcopter [24].

The main drawback of the conventional SMC is the finite-amplitude oscillations in the control signal, the chattering phenomenon, which is caused by the high-frequency switching [2]. Chattering is an undesirable phenomenon because it may excite unmodelled high-frequency plant dynamics resulting in unanticipated instabilities [27]. In addition, it may cause actuator damage or saturation. There exists several methods to reduce the chattering phenomenon such as sigmoid function with a boundary layer [29] and higher-order SMC [32]. Using an adaptive intelligence controller such as fuzzy logic systems and neural networks to estimate the discontinuous sign function is the appropriate techniques to alleviate the chattering issue associated with conventional SMC.

Although in conventional SMC, the sliding surface converges to zero in the finite-time, there is no guarantee that state variables converge to their desired values in finite-time. To solve this problem, terminal sliding mode (TSM) controller is proposed [33]. TSM controller uses a nonlinear sliding surface rather than a linear sliding surface as it is common in conventional SMC. Although in TSM, the convergence of states to their desired values occurs in the finite-time, this type of controller still suffers from singularity problem [18], i.e., the control signal becomes infinite in the vicinity of the desired states. To handle the singularity problem in the TSM controller and enhance the asymptotic convergence rate, nonsingular terminal sliding mode (NTSM) controller and nonsingular fast terminal sliding mode (NFTSM) controller have been proposed [31].

Many practical systems have nonlinearity and uncertainty which make it difficult to control them. Fuzzy inference systems (FISs) can handle these challenges with approximate the uncertain nonlinear functions and optimal gains of controllers [10]. The interval type-2 FIS is developed to better deal with the uncertainty of the control system and increase its robustness. In interval type-2 FIS, all of the crisp membership functions are assumed as an interval; hence the uncertainty can be efficiently handled by the interval membership functions [35]. [19] introduces an adaptive interval type-2 FIS nonsingular fast terminal sliding mode controller with fractional-order manifold for chaotic systems. In [12], a robust dynamic sliding mode controller using interval type-2 FIS is proposed for fuzzy systems based on an asymmetric Lyapunov Krasovskii function.

This type of intelligent controller has different applications in wind prediction, hybrid power systems, and energy storage. The extracting appropriate using the intelligent controller for nodal marginal prices is presented in [1]. The optimal intelligent bidding strategy is introduced for hydrogen storage of electrical vehicles [20]. [34] presents a robust multi-objective strategy of islanded hybrid systems with the renewable and mobile energy source. [25] proposes an intelligent algorithm with hybrid feature selection for wind prediction. In [23], a numerical analysis is investigated for combined and hybrid energy systems containing Stirling engine, thermoelectric device, and dish solar collector. [26] presents a novel and intelligent based predictor for wind-solar and battery output in hybrid power system. A new smart method of bidding and offering for compressed air energy storage is proposed in [5].

- The adaptive fuzzy nonsingular fast terminal sliding mode controller plus a proportionate controller (AFNFTSMC+PC) is introduced to finite-time control and synchronization of a magnetic space-craft chaotic system. The main contributions of the paper are highlighted as follows.
- Adding an adaptive coefficient to the interval type-2 FIS will improve the control system operations in different conditions.
- The novel adaptive switching control term successfully reduces the chattering phenomenon. Also, the transient and steady state tracking error is mitigated.
- The possible singularity associated with NFTSM is alleviated in the proposed control scheme and the finite-time convergence as well as sped up convergence rate is guaranteed in the proposed method.
- Lyapunov stability theorem is used to achieve the adaptation laws for the parameters of the proposed controller and prove the closed-loop stability of the whole system.
- FFT analysis of the control signals, some performance indices, and statistical features are introduced to better comparison between the controller performances.

The simulation results show the effectiveness and robustness of the proposed finite-time controller against chaos behavior, nonlinearity, and parametric uncertainty. In accordance with the obtained results, the AFNFTSMC+PC strategy have a better performance against the adaptive fuzzy controller proposed in [14].

This paper is organized as follows. The formulations and structures of the interval type-2 fuzzy plus proportionate system are given in Section 2. Section 3 presents the nonlinear time-varying model of the magnetic satellite. In Section 4, the numerical simulation results are given, and finally, in the last section, the conclusion of the article is represented.

2 Controller structure

This section presents brief description of the proposed controller and its stability analysis.

The NFTSM controller:

In this subsection, the detailed relations of the NFTSM controller are reviewed. The dynamic model of the nonlinear time-varying system is described as follows.

$$\begin{aligned} \dot{x}_1 =& x_2, \\ \dot{x}_2 =& F(x,t) + u(t), x = [x_1, x_2]^T, \end{aligned} \tag{1}$$

where x is the state vector, $F(x,t)$ is the nonlinear functions and $u(t)$ is the control input. Let the desired state vector be $x_d = [x_{1d}, x_{2d}]$ and the tracking error is defined as follows

$$\begin{aligned} e = x - x_d =& [(x_1 - x_{1d})(x_2 - x_{2d}) = [e_1,\ e_2]^T, \\ \dot{e}_2 =& \dot{x}_2 - \dot{x}_{2d}, \end{aligned} \tag{2}$$

The next move of the controlling problem is to define the TSM and NTSM surfaces as follows

$$\sigma_1 = e_2 + \alpha |e_1|^{\gamma} .sign(e_1), \alpha > 0, 0 < \gamma < 1, \tag{3}$$

$$\sigma_2 = e_1 + \alpha |e_2|^{\gamma} .sign(e_2) \qquad \alpha > 0, \quad 0 < \gamma < 2, \tag{4}$$

σ_1 and σ_2 are the TSM and NTSM surfaces, respectively. If the γ is equal to zero, the TSM is equal linear sliding mode surface, and according to mentioned description stated in the Introduction section, the convergence rate is decreased. The NFTSM surface is represented in (9).

$$\sigma = e_1 + \alpha |e_1|^{\gamma_1} .sign(e_1) + \beta |e_2|^{\gamma_2} .sign(e_2), \quad \alpha > 0, \quad \beta > 0, \quad 1 < \gamma_2 < 2, \quad \gamma_1 > \gamma_2, \tag{5}$$

where σ is the NFTSM surface and α, β, γ_2, γ_1 are the designed parameters. Using the NFTSM surface, the singularity problem in control signal of the TSM controllers has been resolved. The error can converge to zero in the finite-time and it is achieved by the following relation:

$$\dot{e}_1 = -\left(\frac{1}{\beta}\right)^{{\gamma_2}^{-1}} \left(e_1 + \alpha |e_1|^{\gamma_1} .sign(e_1)\right)^{{\gamma_2}^{-1}}, \tag{6}$$

$$\dot{e}_1 = -\left(\frac{1}{\beta}\right)^{{\gamma_2}^{-1}} {e_1}^{{\gamma_2}^{-1}} \left(1 + \alpha |e_1|^{\gamma_1 - 1}\right)^{{\gamma_2}^{-1}}, \tag{7}$$

$$\dot{e}_1 = -\left(\frac{1}{\beta}\right)^{{\gamma_2}^{-1}} \left(e_1 + \alpha |e_1|^{\gamma_1} .sign(e_1)\right)^{{\gamma_2}^{-1}}, \ \dot{e}_1 = -\left(\frac{1}{\beta}\right)^{{\gamma_2}^{-1}} {e_1}^{{\gamma_2}^{-1}} \left(1 + \alpha |e_1|^{\gamma_1 - 1}\right)^{{\gamma_2}^{-1}}.$$

By integrating both sides of (7) over time it obtains

$$\int_{e_1(t_r)}^{e_1(t_r+t_s)} {e_1}^{\gamma_2}\, de_1 = -\int_{t_r}^{t_r+t_s} \left(\frac{1}{\beta}\right)^{{\gamma_2}^{-1}} \left(1 + \alpha |e_1|^{\gamma_1 - 1}\right)^{{\gamma_2}^{-1}} d\tau \ \leq -\int_{t_r}^{t_r+t_s} \left(\frac{1}{\beta}\right)^{{\gamma_2}^{-1}} d\tau, \tag{8}$$

the time convergence of the proposed NFTSM controller is achieved.

$$t_s \leq \frac{\beta^{-(1/\gamma_1)}}{(1 - 1/\gamma_1)} |e_0|^{1-(1/\gamma_1)}, \tag{9}$$

where t_s is the convergence time. The convergence rates when the system states reach the sliding surface ($\sigma = 0$) are illustrated in Fig. 1.

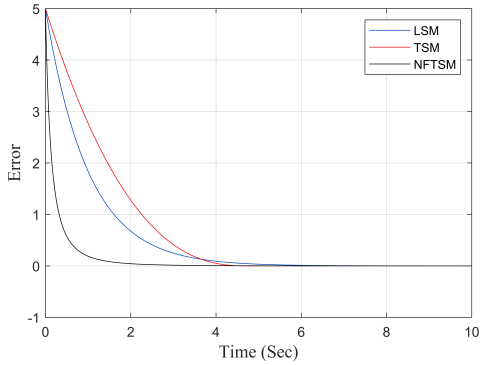


Figure 1: The convergence rate of the surfaces.

The time derivative of the NFTSM surface (9) gives

$$\dot{\sigma} = \dot{e}_1 + \alpha\ \gamma_1 \left|e_1\right|^{\gamma_1 - 1} \dot{e}_1 + \ \beta\ \gamma_2 \left|e_2\right|^{\gamma_2 - 1} \dot{e}_2. \tag{10}$$

The control input of the system includes the two terms of $u_{eq}(t)$ and $u_{sw}(t)$; hence $u(t)$ is found as follows

$$u(t) = u_{eq}(t) + u_{sw}(t). \tag{11}$$

Where $u_{eq}(t)$ denotes the equivalent control term and $u_{sw}(t)$ is the switching control term. If $\dot{\sigma} = 0$, then $u_{eq}(t)$ can be rewritten as:

$$u_{eq}(t) = -\left(\left((\beta\gamma_2)^{-1} \left|e_2\right|^{1-\gamma_2}\right)\left(e_2 + \alpha\ \gamma_1 \left|e_1\right|^{\gamma_1 - 1} e_2\right) + F(x,t) - \dot{x}_{2d}\ \right), \tag{12}$$

and (14) and (15) shows $u_{sw}(t)$

$$u_{sw1}(t) = -\ k_1 \left|\sigma\right|^{\alpha} sign(\sigma), \qquad u_{sw2}(t) = -\ k_2\sigma, \tag{13}$$

$$u_{sw}(t) = u_{sw1}(t) + u_{sw2}(t). \tag{14}$$

Where k_1, k_2 are the design parameters. According to (12)-(14), (15) turns into

$$u(t) = -\left((\beta\gamma_2)^{-1} \left|e_2\right|^{1-\gamma_2}\right)\left(e_2 + \alpha\ \gamma_1 \left|e_1\right|^{\gamma_1 - 1} e_2\right) + F(x,t) - \dot{x}_{2d} + k_1 \left|\sigma\right|^{\alpha} sign(\sigma) + k_2\sigma). \tag{15}$$

Based on (16), (11) is rewritten as

$$\dot{\sigma} = \left(e_2 + \alpha\ \gamma_1 \left|e_1\right|^{\gamma_1 - 1} e_2\right) + \ (\ \beta\gamma_2 \left|e_2\right|^{\gamma_2 - 1})\left(\left((\beta\gamma_2)^{-1} \left|e_2\right|^{1-\gamma_2}\right)\left(e_2 + \alpha\ \gamma_1 \left|e_1\right|^{\gamma_1 - 1} e_2\right)\ + k_1 \left|\sigma\right|^{\alpha} sign(\sigma) + k_2\sigma\right). \tag{16}$$

$$\dot{\sigma} = -\left(\beta\gamma_2 \left|e_2\right|^{\gamma_2 - 1}\right)(k_1 \left|\sigma\right|^{\alpha} sign(\sigma) + k_2\sigma). \tag{17}$$

The candidate Lyapunov function for the stability is expressed as

$$V_1 = \frac{1}{2}\sigma^2. \tag{18}$$

The time derivative of (19) gives

$$\dot{V}_1 = \sigma\dot{\sigma}. \tag{19}$$

From (18), it follows that

$$\dot{V}_1 = -\sigma\ (\beta\gamma_2 \left|e_2\right|^{\gamma_2 - 1})(k_1 \left|\sigma\right|^{\alpha} sign(\sigma) + k_2\sigma). \tag{20}$$

$$\dot{V}_1 = -k_1 \left(\beta\gamma_2 \left|e_2\right|^{\gamma_2 - 1}\right)(\left|\sigma\right|^{\alpha+1}) - k_2(\ \beta\gamma_2 \left|e_2\right|^{\gamma_2 - 1})(\sigma^2). \tag{21}$$

According to (22), when $e_2 \neq 0$, $\dot{V}_1 \leq 0$ and based on Lyapunov theorem, stability of the system is proven if $e_2 = 0$. The state of the system will reach fast to the sliding surface in the finite-time. Substituting (22) into (1) yields

$$\dot{x}_2 = F\left(x,t\right) - \left(\left(\left(\beta\gamma_2\right)^{-1}\left|e_2\right|^{1-\gamma_2}\right)\left(\alpha\ \gamma_1\left|e_1\right|^{\gamma_1 - 1}e_2 + e_2\right) + F\left(x,t\right) - \dot{x}_{2d} + k_1\left|\sigma\right|^{\alpha} sign\left(\sigma\right) + k_2\sigma\right). \tag{22}$$

$$\dot{e}_2 = -\left(\left(\left(\beta\gamma_2\right)^{-1}\left|e_2\right|^{1-\gamma_2}\right)\left(\alpha\ \gamma_1\left|e_1\right|^{\gamma_1 - 1}e_2 + e_2\right) + k_1\left|\sigma\right|^{\alpha} sign\left(\sigma\right) + k_2\sigma\right). \tag{23}$$

With respect to $e_2 = 0$, (24) can be rewritten as

$$\dot{e}_2 = -\left(k_1\left|\sigma\right|^{\alpha} sign\left(\sigma\right) + k_2\sigma\right). \tag{24}$$

If $\sigma > 0$, then $\dot{e}_2 < k_1$ and if $\sigma < 0$, then $\dot{e}_2 > k_1$. According to [7], $\dot{e}_2$ is not an attractor. Additionally, there is a vicinity of $e_2 = 0$, i.e $\left|e_2\right| \leq \delta$, satisfying $\dot{e}_2 < k_1$ for $\sigma > 0$ and $\dot{e}_2 > k_1$ for $\sigma < 0$. Therefore, the trajectory cross the two boundary of the vicinity ($\left|e_2\right| \leq \delta$) in the finite-time and according to (25) in the other region i.e., $\left|e_2\right| \geq \delta$, the system states reached the surface in the finite-time [36].

The structure of the proposed FIS:

The FIS contains four parts which are fuzzifier, rule base, inference engine, and defuzzifier [16]. In the inference engine combines rules using product t-norm as follows:

$$A^j = \prod_{i=1}^{n} \mu_{A_i^j}\left(x_i\right), \tag{25}$$

where $\mu_{A_i^j}$ is the MFs grades for the x_i, i is the index of input, and A^j is the product of the grades. In an interval type-2 FIS, each interval type-2 MF in the antecedent part has a lower and an upper MF which compose an interval fuzzy rule with their upper and lower bounds as follows:

$$\overline{A}^j = \prod_{i=1}^{n} \overline{\mu}_{A_i^j}\left(x_i\right), \tag{26}$$

$$\underline{A}^j = \prod_{i=1}^{n} \underline{\mu}_{A_i^j}\left(x_i\right), \tag{27}$$

where $\overline{\mu}_{A_i^j}$ and $\underline{\mu}_{A_i^j}$ are the upper and lower MFs grades for the x_i and $\overline{A}^j$ and $\underline{A}^j$ are the product of the membership grades, respectively. The normalized vector of $\overline{A}^j$and $\underline{A}^j$ are shown in (28) and (29).

$$\zeta_U = \frac{\sum_{i=1}^{M}\left(\left(\overline{A}_i + \underline{A}_i\right) + A_i sign\left(\overline{m}_i\right)\right)}{\sum_{i=1}^{M}\left(\overline{A}_i + \underline{A}_i\right) + \sum_{i=1}^{M}\left(sign\left(\overline{m}_i\right)\Delta A_i\right)}, \tag{28}$$

$$\zeta_L = \frac{\sum_{i=1}^{M}\left(\left(\overline{A}_i + \underline{A}_i\right) + A_i\left(sgn\left(\underline{m}_i\right)\right)\right)}{\sum_{i=1}^{M}\left(\overline{A}_i + \underline{A}_i\right) + \sum_{i=1}^{M}\left(sgn\left(\underline{m}_i\right)\Delta A_i\right)}, \tag{29}$$

where ζ_U and ζ_L are the normalized vector of $\overline{A}^j$ and $\underline{A}^j$, respectively, and $\underline{m}_i$, $\overline{m}_i$, δ and ΔA can be expressed as

$$\overline{m}_i = \overline{W}_i - \frac{\sum_{i=1}^{M}\overline{A}_i\overline{W}_i}{\sum_{i=1}^{M}\overline{A}_i}, \tag{30}$$

$$\underline{m}_i = \underline{W}_i - \frac{\sum_{i=1}^{M}\underline{A}_i\underline{W}_i}{\sum_{i=1}^{M}\underline{A}_i}. \tag{31}$$

$$\Delta A_i = \overline{A}_i - \underline{A}_i. \tag{32}$$

The upper and lower output of the interval type-2 FIS based on Mamdani inference system and center of sets type reduction followed by defuzzification (COS TR + D) [15] is expressed as in (34) and (35).

$$Y_U = \frac{\sum_{i=1}^{M} \left(\left(\overline{A}_i + \underline{A}_i\right) + A_i \left(sgn\left(\overline{m}_i\right)\right)\right) \overline{W}_i}{\sum_{i=1}^{M} \left(\overline{A}_i + \underline{A}_i\right) + \sum_{i=1}^{M} \left(sgn\left(\overline{m}_i\right) A_i\right)}. \tag{33}$$

$$Y_L = \frac{\sum_{i=1}^{M} \left(\left(\overline{A}_i + \underline{A}_i\right) + A_i \left(sgn\left(\underline{m}_i\right)\right)\right) \underline{W}_i}{\sum_{i=1}^{M} \left(\overline{A}_i + \underline{A}_i\right) + \sum_{i=1}^{M} \left(sgn\left(\underline{m}_i\right) A_i\right)}, \tag{34}$$

where Y_U and Y_L are the upper and lower outputs of the interval type-2 FIS, $\overline{W}_i$ and $\underline{W}_i$ are the upper and lower centers of the consequent part MFs, with respect to (36) and (37) and summarizing (34) and (35), we can get

$$Y_U = \overline{W}^T \zeta_U, \tag{35}$$

$$Y_L = \underline{W}^T \zeta_L, \tag{36}$$

$$Y = 0.5 \left(Y_U + Y_L\right), \tag{37}$$

where Y is the output of interval type-2 FIS. In this paper, a constant value is added to output of the interval type-2 FIS to add more degrees of freedom to it. The bias factor has the effect of applying affine transformation to the output of interval type-2 FIS. Equation (46) illustrates the output of the proposed interval type-2 FIS plus proportionate bias.

$$Y = 0.5 * \left(Y_L + Y_U\right) + B. \tag{38}$$

Adaptive fuzzy nonsingular fast terminal sliding mode controller plus a proportionate controller (AFNFTSMC+PC):

In this subsection, the formula, structure, and stability analysis of the proposed AFNFTSMC+PC is illustrated. In this work, in order to attenuate the chattering phenomenon, the discontinuous part of the switching control term $(u_{sw1}(t))$ has been replaced with an interval type-2 FIS plus a proportional controller. Moreover, the gain of k_2 in $u_{sw2}(t)$ is considered as an adaptive parameter during the whole procedure. The error vector is determined as the fuzzy input and its corresponding output is the estimated values of u_{sw1} and k_2.

$$\hat{u}_{sw1} = \widehat{\overline{W}}_s^T \zeta_U + \widehat{\underline{W}}_s^T \zeta_L \ + \hat{B}_s, \tag{39}$$

$$\hat{k}_2 = \widehat{\overline{W}}_k^T \zeta_U + \widehat{\underline{W}}_k^T \zeta_L + \hat{B}_k, \tag{40}$$

where $\widehat{\underline{W}}_s$, $\widehat{\overline{W}}_s$, $\widehat{\underline{W}}_k$ and $\widehat{\overline{W}}_k$ are the estimated weights of proportionate term in the consequent part of the controller, respectively. The optimal values of the weights in the consequent part of the interval type-2 FIS plus proportionate are defined as follows

$$\left(\overline{W}_s^*, \underline{W}_s^*, B_s^*\right) = \ arg \ \ min \ [\ sup \ |\hat{u}_{sw1} - u_{sw1}^*|], \tag{41}$$

$$\left(\overline{W}_k^*, \underline{W}_k^*, B_k^*\right) = arg \ \ min \ \left[\ sup \ \left|\hat{k}_2 - k_2^*\right|\right], \tag{42}$$

where $\overline{W}_s^*$, $\underline{W}_s^*$ and B_s^* are the optimal weights corresponding to $u_{sw1}(t)$ and $\overline{W}_k^*$, $\underline{W}_k^*$ and B_k^* denotes the optimal weights of k_2 in the interval type-2 FIS plus proportionate. The optimal values of the u_{sw1} and k_2 are given as follows:

$$u_{sw1}^* = \overline{W}_s^{*T} \zeta_U + \underline{W}_s^{*T} \zeta_L + B_s^*, \tag{43}$$

$$k_2^* = \overline{W}_k^{*T}\zeta_U + \underline{W}_k^{*T}\zeta_L + B_k^*, \tag{44}$$

the error estimations of $u_{sw1}(t)$ and k_2 of the are expressed in (46-47).

$$\widetilde{u}_{sw1} = \hat{u}_{sw1} - \ u_{sw1}^*, \tag{45}$$

$$\widetilde{k}_2 = \hat{k}_2 - \ k_2^*, \tag{46}$$

(48-49) expresses the error estimations of the adaptive parameters.

$$\widetilde{W} = \hat{W} - W^*, \tag{47}$$

$$\widetilde{B} = \hat{B} - B^*, \tag{48}$$

where $\widetilde{W}$ and $\widetilde{B}$ are the error estimation values of the weights and biases, respectively. By substituting the estimated values of $u_{sw1}(t)$ and k_2 into (18) yields

$$\dot{\sigma} = -(\ \beta\gamma_2\,|e_2|^{\gamma_2-1})(\hat{u}_{sw1}) - (\hat{k}_2)(\ \beta\gamma_2\,|e_2|^{\gamma_2-1})\sigma. \tag{49}$$

The substituting (47-48) into (57) gives

$$\dot{\sigma} = -(\ \beta\gamma_2\,|e_2|^{\gamma_2-1})(\widehat{\overline{W}}_s^T\zeta_U + \widehat{\underline{W}}_s^T\zeta_L + \hat{B}_s) - (\widehat{\overline{W}}_k^T\zeta_U + \widehat{\underline{W}}_k^T\zeta_L + \hat{B}_k)(\ \beta\gamma_2\,|e_2|^{\gamma_2-1})\sigma. \tag{50}$$

The candidate Lyapunov function to prove the stability of the system is expressed as

$$V_2 = \frac{1}{2}\sigma^2 + \frac{1}{\eta}\widetilde{\underline{W}}_k^T\widetilde{\underline{W}}_k + \frac{1}{\eta}\widetilde{\overline{W}}_k^T\widetilde{\overline{W}}_k + \frac{1}{\eta}\widetilde{\underline{W}}_s^T\widetilde{\underline{W}}_s + \frac{1}{\eta}\widetilde{\overline{W}}_s^T\widetilde{\overline{W}}_s + \frac{1}{\eta}\widetilde{B}_k\widetilde{B}_k \ + \ \frac{1}{\eta}\widetilde{B}_s\widetilde{B}_s, \tag{51}$$

where η is the adaptation rate and must be positive. Taking the time derivative of (59) yields

$$\dot{V}_2 = \sigma\dot{\sigma} + \frac{2}{\eta}\widetilde{\underline{W}}_k^T\dot{\widehat{\underline{W}}}_k + \frac{2}{\eta}\widetilde{\overline{W}}_k^T\dot{\widehat{\overline{W}}}_k + \frac{2}{\eta}\widetilde{\underline{W}}_s^T\dot{\widehat{\underline{W}}}_s + \frac{2}{\eta}\widetilde{\overline{W}}_s^T\dot{\widehat{\overline{W}}}_s + \ \ \frac{2}{\eta}\widetilde{B}_k\dot{\hat{B}}_k + \ \ \frac{2}{\eta}\widetilde{B}_s\dot{\hat{B}}_s. \tag{52}$$

By substituting the expression in (58) in (60), the following equation is obtained.

$$\dot{V}_2 = -\sigma\ \left((\ \beta\gamma_2\,|e_2|^{\gamma_2-1})(\widehat{\underline{W}}_s^T\zeta_L + \widehat{\overline{W}}_s^T\zeta_U + \hat{B}_s) - \left(\widehat{\underline{W}}_k^T\zeta_L + \widehat{\overline{W}}_k^T\zeta_U + \hat{B}_s\right)\left(\beta\gamma_2\,|e_2|^{\gamma_2-1}\right)\sigma\right) + \tag{53}$$
$$\frac{2}{\eta}\widetilde{\underline{W}}_k^T\dot{\widehat{\underline{W}}}_k + \frac{2}{\eta}\widetilde{\overline{W}}_k^T\dot{\widehat{\overline{W}}}_k + \frac{2}{\eta}\widetilde{\underline{W}}_s^T\dot{\widehat{\underline{W}}}_s + \frac{2}{\eta}\widetilde{\overline{W}}_s^T\dot{\widehat{\overline{W}}}_s + \ \ \frac{2}{\eta}\widetilde{B}_k\dot{\hat{B}}_k + \ \ \frac{2}{\eta}\widetilde{B}_s\dot{\hat{B}}_s,$$

(60) is divided into the two parts of $\dot{V}_{2-1}$ and $\dot{V}_{2-2}$ (62-63).

$$\dot{V}_{2-1} = -\sigma\left(\ \beta\gamma_2\,|e_2|^{\gamma_2-1}\right)\left(\widehat{\underline{W}}_s^T\zeta_L - \underline{W}_s^{*T}\zeta_L + \widehat{\overline{W}}_s^T\zeta_U - \overline{W}_s^{*T}\zeta_U + \underline{W}_s^{*T}\zeta_L + \overline{W}_s^{*T}\zeta_U + \hat{B}_s - B_s^* + B_s^*\right) + \tag{54}$$
$$\frac{2}{\eta}\widetilde{\underline{W}}_s^T\dot{\widehat{\underline{W}}}_s + \frac{2}{\eta}\widetilde{\overline{W}}_s^T\dot{\widehat{\overline{W}}}_s + \frac{2}{\eta}\widetilde{B}_s\dot{\hat{B}}_s.$$

$$\dot{V}_{2-2} = -\sigma^2\left(\ \beta\gamma_2\,|e_2|^{\gamma_2-1}\right)\left(\widehat{\underline{W}}_k^T\zeta_L - \underline{W}_k^{*T}\zeta_L + \widehat{\overline{W}}_k^T\zeta_U - \overline{W}_k^{*T}\zeta_U + \underline{W}_k^{*T}\zeta_L + \overline{W}_k^{*T}\zeta_U + \hat{B}_k - B_k^* + B_k^*\right) + \tag{55}$$
$$\frac{2}{\eta}\widetilde{\underline{W}}_k^T\dot{\widehat{\underline{W}}}_k + \frac{2}{\eta}\widetilde{\overline{W}}_k^T\dot{\widehat{\overline{W}}}_k + \frac{2}{\eta}\widetilde{B}_k\dot{\hat{B}}_k.$$

The adaptation laws are taken to satisfy the (55) and (56).

$$-\sigma(\ \beta\gamma_2\,|e_2|^{\gamma_2-1})(\widetilde{\underline{W}}_s^T\zeta_L + \widetilde{\overline{W}}_s^T\zeta_U + \widetilde{B}_s) + \frac{2}{\eta}\widetilde{\underline{W}}_s^T\dot{\widehat{\underline{W}}}_s + \frac{2}{\eta}\widetilde{\overline{W}}_s^T\dot{\widehat{\overline{W}}}_s + \frac{2}{\eta}\widetilde{B}_s\dot{\hat{B}}_s \ = 0. \tag{56}$$

$$-\sigma^2(\ \beta\gamma_2\,|e_2|^{\gamma_2-1})(\widetilde{\underline{W}}_k^T\zeta_L+\widetilde{\overline{W}}_k^T\zeta_U+\widetilde{B}_k)+\frac{2}{\eta}\widetilde{\underline{W}}_k^T\dot{\underline{\widehat{W}}}_k+\frac{2}{\eta}\widetilde{\overline{W}}_k^T\dot{\overline{\widehat{W}}}_k+\frac{2}{\eta}\widetilde{B}_k\dot{\hat{B}}_k=0. \tag{57}$$

Hence the control law (adaptation rule) is defined as

$$\dot{\underline{\widehat{W}}}_s=\ \frac{\eta}{2}\sigma(\ \beta\gamma_2\,|e_2|^{\gamma_2-1})\zeta_L, \tag{58}$$

$$\dot{\overline{\widehat{W}}}_s=\ \frac{\eta}{2}\sigma(\ \beta\gamma_2\,|e_2|^{\gamma_2-1})\zeta_U, \tag{59}$$

$$\dot{\hat{B}}_s=\ \frac{\eta}{2}\sigma(\ \beta\gamma_2\,|e_2|^{\gamma_2-1}), \tag{60}$$

$$\dot{\underline{\widehat{W}}}_k=\ \frac{\eta}{2}\sigma^2(\ \beta\gamma_2\,|e_2|^{\gamma_2-1})\zeta_L, \tag{61}$$

$$\dot{\overline{\widehat{W}}}_k=\ \frac{\eta}{2}\sigma^2(\ \beta\gamma_2\,|e_2|^{\gamma_2-1})\zeta_U, \tag{62}$$

$$\dot{\hat{B}}_k=\ \frac{\eta}{2}\sigma^2(\ \beta\gamma_2\,|e_2|^{\gamma_2-1}). \tag{63}$$

Based on (59-64), (54) can be rewritten as

$$\dot{V}_2=-\sigma\left(\ \beta\gamma_2\,|e_2|^{\gamma_2-1}\right)\left(\underline{W}_s^{*T}\zeta_L+\overline{W}_s^{*T}\zeta_U+B_s^*\right)-\sigma^2\left(1+\ \beta\gamma_2\,|e_2|^{\gamma_2-1}\right)\left(\underline{W}_k^{*T}\zeta_L+\overline{W}_k^{*T}\zeta_U+B_k^*\right). \tag{64}$$

By using the optimal values of u_{sw1} and k_2 and with respect to (28-31) the stability of the system in a Lyapunov sense is proven and we have the following inequality for the time derivative of the Lyapunov function.

$$\dot{V}_2\leq 0. \tag{65}$$

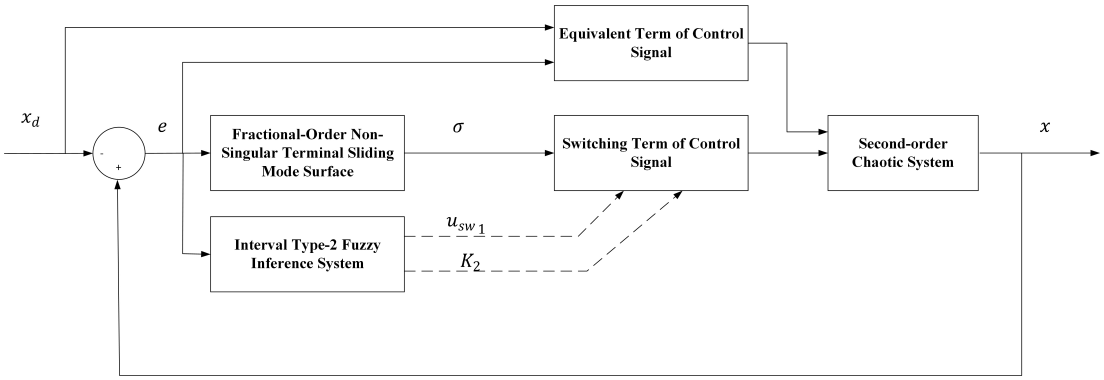


Figure 2: The block diagram of the proposed AFNFTSMC+PC for the second-order chaotic system.

3 System description

The magnetic rigid satellite moves in a circular orbit with the orbital angular velocity ω_c in the magnetic fields of the Earth affected by the Earths gravity. The inertial reference frame (O_e-$X_0Y_oZ_o$) contains the origin O_e at the mass center of the Earth. The two main axes are the polar axis as Z_o-axis and the line from O_e to the ascending node as X_o-axis. Let us define ($O_e - XYZ$) as the orbital reference frame so that X and Z are in the anti-nadir direction

and the normal vector of the orbital plane XY direction, respectively [14]. The dynamic model of the magnetic rigid satellite is presented in (67).

$$\begin{aligned} \dot{x}_1 =& x_2 \\ \dot{x}_2 =& -K\sin(2x_1) - \gamma x_2 - \alpha_s\left(2\sin(x_1)\sin(t) + \cos(x_1)\cos(t)\right) + u(t), \end{aligned} \tag{66}$$

where x_1 is the libration angle that denotes the deviation of the satellite-fixed x axis and y axis, α_s is the magnetic parameter, γ is the damping parameter and K is determined as

$$K = \frac{3(B-A)}{2C}, \tag{67}$$

where A, B and C represent the inertia moments of the satellite. In this paper, K is equal to 1.1. The phase portrait of the system for the nominal parameters $\gamma = 0.29$, $\alpha_s = 0.7$ and initial values of $x_1(0)$=-0.5, $x_2(0)$=0.25 is illustrated in Fig.3.

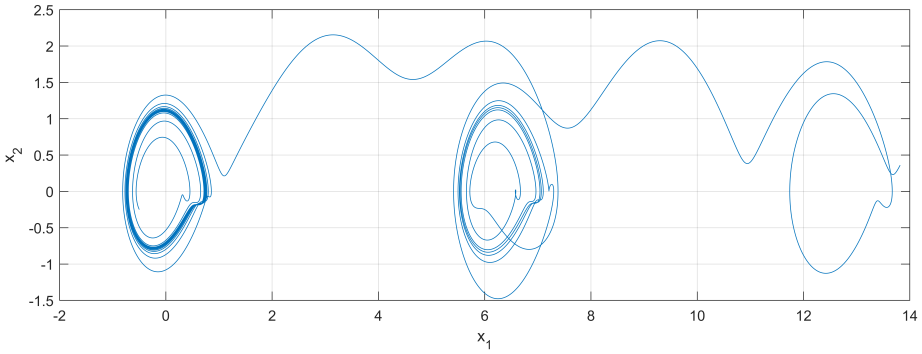


Figure 3: The phase portrait of the magnetic rigid satellite nominal values and initial conditions $x_1(0) = -0.5$, $x_2(0) = 0.25$.

4 Simulation results

The proposed chattering free controller is applied to control the magnetic space-craft with the step and the sinusoidal input and synchronizing with the duffing oscillation system. Three different scenarios have been investigated to illustrate the superiority of the proposed controller against other methods, i.e., the SM, NTSM, NFTSM, AFNFTSM controllers and AFNFTSMC+PC. The system first must be synchronized with the duffing force oscillation system in the first 30 seconds. Then in the next 5 seconds, the systems must converge to zero ($x_1(t) = 0$,$x_2(t) = 0$) and finally, the system should track the sinusoidal input with the frequency 10 rad/sec and the amplitude 1. The state-space of the duffing force oscillation system is presented in (69).

$$\begin{aligned} \dot{x}_1 =& x_2, \\ \dot{x}_2 =& -0.1x_2 - x_1^3 + 12\cos(t). \end{aligned} \tag{68}$$

Details of the magnetic space-craft system simulation scenarios are given as follows [14].

- Initial conditions are $x_1(0) = -0.6$, $x_2(0) = -0.6$ with the $\gamma = 0.29$, $\alpha_s = 0.6984$, initial conditions of the duffing force oscillation system are $x_1(0) = 1$, $x_2(0) = 3$.
- Initial conditions are $x_1(0) = -0.5$, $x_2(0) = -0.25$ with the $\gamma = 0.29$, $\alpha_s = 0.7$, initial conditions of the duffing force oscillation system are $x_1(0) = 0.5$, $x_2(0) = -3.7$.
- Initial conditions are $x_1(0) = 0.4$, $x_2(0) = -0.75$ with the $\gamma = 0.297$, $\alpha_s = 0.7$, initial conditions of the duffing force oscillation system are $x_1(0) = 2.5$, $x_2(0) = 1$.
- FFT analysis of the control signals, some performance indices, and statistical features are introduced to better comparison between the controller performances.

With respect to details of the three scenarios, the robustness of the proposed AFNFTSMC+PC against the nominal parameter and initial condition variations will be examined. The values of the controller parameters in the simulation scenarios are sets as $\lambda_1 = 1.87$, $\gamma_2 = 1$, $\gamma_1 = 1.57$, $\eta = 0.26$, $k_1 = 20.6$, and $k_2 = 7.9$. These parameters are achieved by trial and error in the first scenario and have not been changed in the next two scenarios. Figs (4-9) show the simulation results for these initial conditions.

According to the time and frequency domain analysis of the control signal, the chattering of the proposed approach has dropped dramatically, due to the use of interval type-2 FIS. By adding a proportional controller in parallel to the interval type-2 FIS, the chattering phenomenon is reduced and the convergence rate is increased. Additionally, the FFT analysis of the control signal indicates that the proposed control signal is a smooth one. Therefore, the controller performance has not deteriorated and is still acceptable. Considering the control signals, no singularity occurs in the control signals when the NFTSM surface reaches zero in the finite-time. The proposed controller has a robust performance against parameter variations with different initial conditions. The performance indices such as IAE and ISE for five different controllers including the proposed approach are presented in Table 1. According to the reasons mentioned in the Introduction section, the control and synchronization of chaotic systems require high accuracy in error tracking. As the simulation results, despite the increased complexity in the AFNFTSMC+PC with interval type-2 FIS structure, it dramatically increases the tracking accuracy. Also, this controller has drastically reduced the chattering phenomenon.

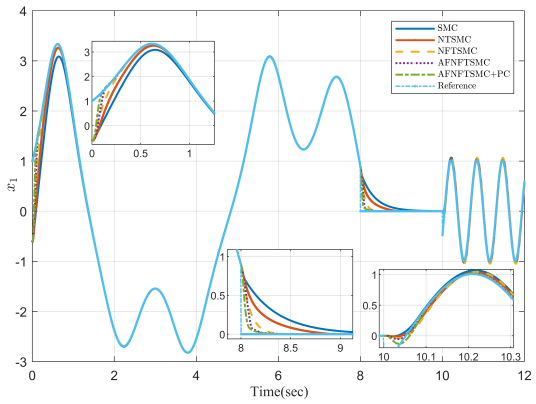


Figure 4: Trajectory of x_1 using SMC, NTSMC, NFTSMC, AFNFTSMC and AFNFTSMC+PC in the first scenario of the magnetic space-craft system.

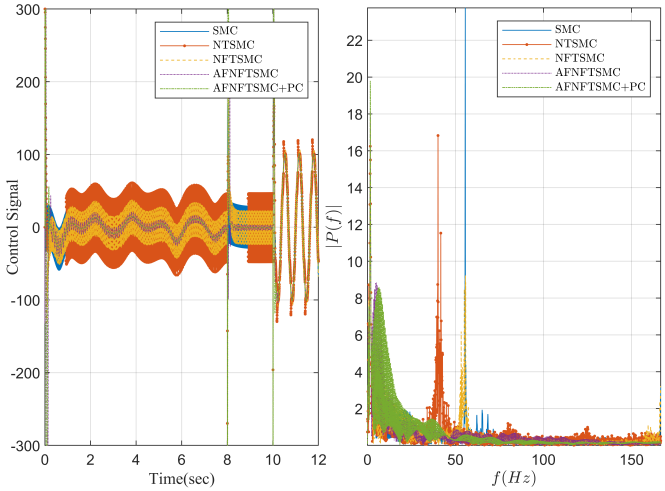


Figure 5: Control signals and its FFT analysis of SMC, NTSMC, NFTSMC, AFNFTSMC and AFNFTSMC+PC in the first scenario of the magnetic space-craft system.

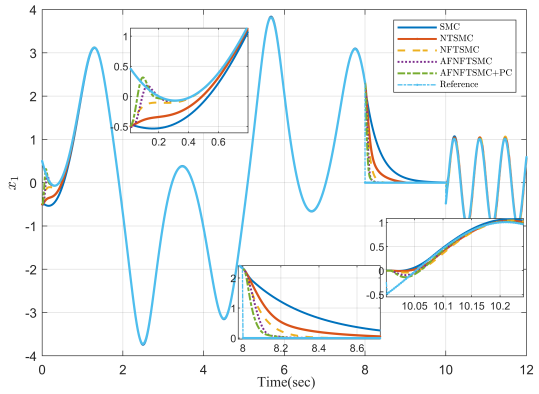


Figure 6: Trajectory of x_1 using SMC, NTSMC, NFTSMC, AFNFTSMC and AFNFTSMC+PC in the second scenario of the magnetic space-craft system.

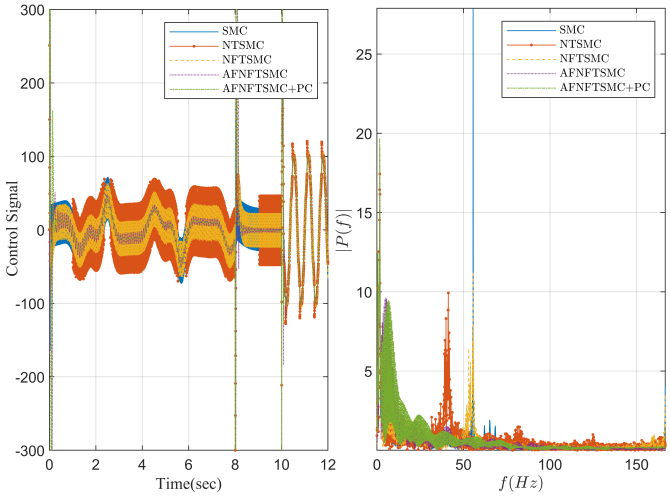


Figure 7: Control signals and its FFT analysis of SMC, NTSMC, NFTSMC, AFNFTSMC and AFNFTSMC+PC in the second scenario of the magnetic space-craft system.

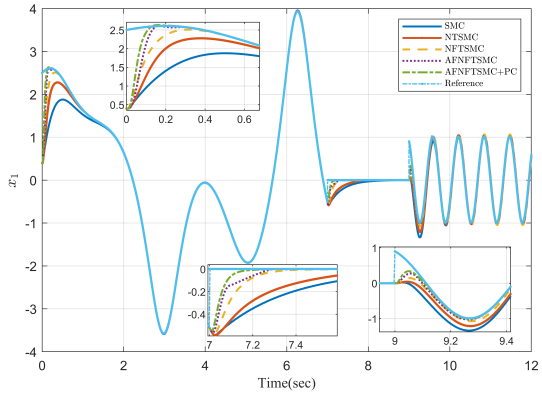


Figure 8: Trajectory of x_1 using SMC, NTSMC, NFTSMC, AFNFTSMC and AFNFTSMC+PC in the third scenario of the magnetic space-craft system.

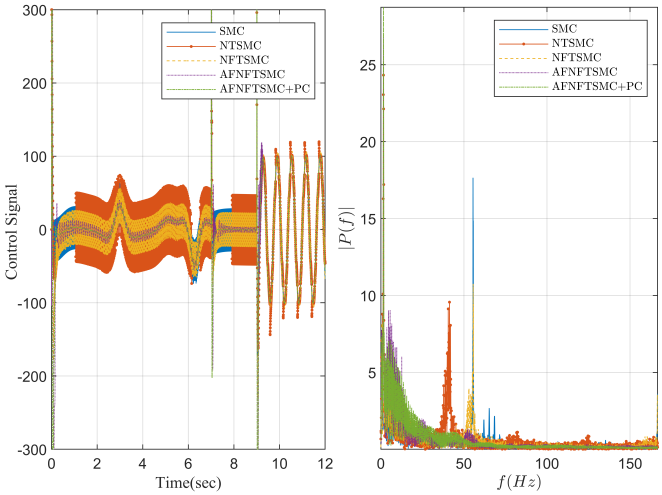


Figure 9: Control signals and its FFT analysis of SMC, NTSMC, NFTSMC, AFNFTSMC and AFNFTSMC+PC in the third scenario of the magnetic space-craft system.

Table 1: Error performance indices for different scenarios using SMC, NTSMC, NFTSMC, AFNFTSMC and AFNFTSMC+PC

	IAE (1st)	ISE (1st)	IAE (2nd)	ISE (2nd)	IAE (3rd)	ISE (3rd)
SMC	1.4679	0.4585	1.4355	0.4644	1.3316	0.3840
NTSMC	1.0982	0.3161	1.0769	0.2997	0.9987	0.2626
NFTSMC	0.9746	0.1899	0.9637	0.1818	0.9273	0.1639
AFNFTSMC	0.8421	0.1212	0.6978	0.1299	0.7145	0.1303
AFNFTSMC + PC	0.6149	0.0837	0.4923	0.0786	0.3796	0.0702

Considering Table 1, the AFNFTSMC+PC shows improved performance in convergence rate. Also, the average and variance of the error have been reduced using AFNFTSMC+PC compared with the conventional one. Additionally, some performance indices such as Control Energy (CE) and Average Chattering Magnitude (ACM) which is related to the control signals have been utilized for better comparison between the controllers. (69) and (70) gives the CE and ACM formulas.

$$CE = \int_0^{Ts} \left(u^2\right) dt, \tag{69}$$

$$ACM = \left(RMS\left(\sqrt{x^2} - \sqrt{x_d^2}\right)\right). \tag{70}$$

As seen in (69) and (70), these performance indices are based on statistical features. These features are presented in Table 2.

Table 2: Error performance indices for different scenarios using SMC, NTSMC, NFTSMC, AFNFTSMC and AFNFTSMC+PC

	CE (1st)	ACM (1st)	CE (2nd)	ACM (2nd)	CE (3rd)	ACM (3rd)
SMC	49841	4.7892e-03	56843	8.1373e-03	56794	5.1561e-03
NTSMC	42613	1.4679e-03	51186	6.6423e-03	52318	3.1236e-03
NFTSMC	35619	7.4512e-04	43431	1.9722e-03	46843	9.0439e-04
AFNFTSMC	26641	3.9742e-04	36464	7.1760e-04	37137	4.1783e-04
AFNFTSMC + PC	23546	2.0077e-04	29463	5.0046e-04	28941	3.3778e-04

According to the performance indices stated in Table 2, the proposed AFNFTSMC+PC has a smooth behavior in the presence of the chaotic behavior and uncertainty; hence it provides a more suitable control signal in comparison

with the other controllers. Also, the variance of the control signal is highly related to the chattering phenomenon; hence by reducing the chattering phenomenon, the variance of the control signal is also reduced.

5 Conclusions

This study introduces a control scheme that benefits from interval type-2 FIS plus a proportional controller acting in parallel to it for control and synchronization of the second-order nonlinear time-varying chaotic systems in the presence of uncertainty. This control strategy is designed to integrate the benefits of the NFTSM controller and the interval type-2 FIS acting in parallel with a proportional controller. The adaptation rule of the proposed structure is derived from a Lyapunov stability theorem.

Simulation results demonstrate that the proposed controller successfully increases the convergence rate, eliminates the singularity, and reduces the chattering of the conventional TSM controller with lower control costs. Even though slight changes in the nominal parameters and initial conditions enormously influence the state trajectories of the system, but the proposed AFNFTSMC+PC can suppress it. In other words, it is observed that the performance of the closed-loop system is independent of the nominal parameters and initial conditions.

The closed-loop stability is proven with the proposed control law. Moreover, the results confirm the claim that by adding adaptive proportionate controller to the interval type-2 FIS, the flexibility and performance of the control system was enhanced.

Future research will be focused on the alleviation of the chattering phenomenon by adaptive fractional-order dynamic sliding mode with fast nonsingular terminal sliding manifold and adaptive fractional-order with deep reinforcement learning method.

References

[1] P. Akbary, M. Ghiasi, M. R. R. Pourkheranjani, H. Alipour, N. Ghadimi, *Extracting appropriate nodal marginal prices for all types of committed reserve*, Computational Economics, **53**(1) (2019), 1-26.

[2] R. K. Amirabadi, O. S. Fard, A. Mansoori, *A novel fuzzy sliding mode control approach for chaotic systems*, Iranian Journal of Fuzzy Systems, **18**(6) (2021), 133-150.

[3] M. H. Barhaghtalab, S. Mobayen, F. Merrikh-Bavat, *Design of a global sliding mode controller using hyperbolic functions for nonlinear systems and application in chaotic systems*, ICEE 2019 - 27th Iranian Conference on Electrical Engineering, (2019), 1030-1034.

[4] M. Boukattaya, N. Mezghani, T. Damak, *Adaptive nonsingular fast terminal sliding-mode control for the tracking problem of uncertain dynamical systems*, ISA Transactions, **77** (2018), 1-19.

[5] W. Cai, R. Mohammaditab, G. Fathi, K. Wakil, A. G. Ebadi, N. Ghadimi, *Optimal bidding and offering strategies of compressed air energy storage: A hybrid robust-stochastic approach*, Renewable Energy, **143** (2019), 1-8.

[6] F. Farivar, M. A. Shoorehdeli, M. A. Nekoui, M. Teshnehlab, *Chaos synchronization of uncertain nonlinear gyros via hybrid control*, IEEE/ASME International Conference on Advanced Intelligent Mechatronics, AIM, **1** (2009), 1365-1370.

[7] Y. Feng, X. Yu, Z. Man, *Non-singular terminal sliding mode control of rigid manipulators*, Automatica, **38**(12) (2002), 2159-2167.

[8] K. Hooshmandi, F. Bayat, M. Jahedmotlagh, A. Jalali, *Guaranteed cost nonlinear sampled-data control: Applications to a class of chaotic systems*, Nonlinear Dynamics, **100** (2020), 731-748.

[9] J. Huang, J. Yang, D. Xie, D. Wu, *Optimal sliding mode chaos control of direct-drive wave power converter*, IEEE Access, **7** (2019), 90922-90930.

[10] Y. Jin, W. Cao, M. Wu, Y. Yuan, *Data-based variable universe adaptive fuzzy controller with self-tuning parameters*, Applied Soft Computing, **123** (2022), 108944.

[11] S. Johari, M. Yaghoobi, H. R. Kobravi, *Nonlinear model predictive control based on hyper chaotic diagonal recurrent neural network*, Journal of Central South University, **29**(1) (2022), 197-208.

[12] R. Kavikumar, B. Kaviarasan, Y. G. Lee, O. M. Kwon, R. Sakthivel, S. G. Choi, *Robust dynamic sliding mode control design for interval type-2 fuzzy systems*, Discrete and Continuous Dynamical Systems, **15**(7) (2022), 1839.

[13] R. Khalili Amirabadi, O. S. Fard, A. Mansoori, *A novel fuzzy sliding mode control approach for chaotic systems*, Iranian Journal of Fuzzy Systems, **18**(6) (2021), 133-150.

[14] M. A. Khanesar, E. Kayacan, M. Reyhanoglu, O. Kaynak, *Feedback error learning control of magnetic satellites using type-2 fuzzy neural networks with elliptic membership functions*, IEEE Transactions on Cybernetics, **45**(4) (2015), 858-868.

[15] M. A. Khanesar, J. M. Mendel, *Maclaurin series expansion complexity-reduced center of sets type-reduction + defuzzification for interval type-2 fuzzy systems*, 2016 IEEE International Conference on Fuzzy Systems, no. D, (2016), 1224-1231.

[16] M. A. L. Khaniki, M. B. Hadi, M. Manthouri, *Tuning of novel fractional order fuzzy PID controller for automatic voltage regulator using grasshopper optimization algorithm*, Majlesi Journal of Electrical Engineering, **15**(2) (2021), 39-45.

[17] S. Kumar, A. E. Matouk, H. Chaudhary, S. Kant, *Control and synchronization of fractionalorder chaotic satellite systems using feedback and adaptive control techniques*, International Journal of Adaptive Control and Signal Processing, **35**(4) (2021), 484-497.

[18] M. A. Labbaf Khaniki, M. Salehi Kho, M. Aliyari Shoorehdeli, *Control and synchronization of chaotic spur gear system using adaptive non-singular fast terminal sliding mode controller*, Transactions of the Institute of Measurement and Control, **44**(14) (2022). DOI:10.1177/01423312221087578.

[19] M. A. Labbaf Khaniki, M. TavakoliKakhki, *Adaptive type-II fuzzy nonsingular fast terminal sliding mode controller using fractionalorder manifold for secondorder chaotic systems*, Asian Journal of Control, **26**(3) (2021), 2653.

[20] J. Liu, C. Chen, Z. Liu, K. Jermsittiparsert, N. Ghadimi, *An IGDT-based risk-involved optimal bidding strategy for hydrogen storage-based intelligent parking lot of electric vehicles*, Journal of Energy Storage, **27** (2020), 101057.

[21] H. F. Löchel, D. Eger, T. Sperlea, D. Heider, J. Wren, *Deep learning on chaos game representation for proteins*, Bioinformatics, **36**(1) (2020), 272-279.

[22] H. Medhaffar, M. Feki, N. Derbel, *Stabilization of chaotic systems via fuzzy time-delayed controller approach*, Iranian Journal of Fuzzy Systems, **16**(2) (2019), 17-29.

[23] M. Mehrpooya, N. Ghadimi, M. Marefati, S. A. Ghorbanian, *Numerical investigation of a new combined energy system includes parabolic dish solar collector, Stirling engine and thermoelectric device*, International Journal of Energy Research, **45**(11) (2021), 16436-16455.

[24] N. Miladi, H. Dimassi, S. Hadj Said, F. M'Sahli, *Explicit nonlinear model predictive control tracking control based on a sliding mode observer for a quadrotor subject to disturbances*, Transactions of the Institute of Measurement and Control, **42**(2) (2020), 214-227.

[25] M. Mir, M. Shafieezadeh, M. A. Heidari, N. Ghadimi, *Application of hybrid forecast engine based intelligent algorithm and feature selection for wind signal prediction*, Evolving Systems, **11**(4) (2020), 559-573.

[26] F. Mirzapour, M. Lakzaei, G. Varamini, M. Teimourian, N. Ghadimi, *A new prediction model of battery and wind-solar output in hybrid power system*, Journal of Ambient Intelligence and Humanized Computing, **10**(1) (2019), 77-87.

[27] S. Mondal, C. Mahanta, *Adaptive second order terminal sliding mode controller for robotic manipulators*, Journal of the Franklin Institute, **351**(4) (2014), 2356-2377.

[28] O. Solaymani Fard, R. Khalili, A. Mansoori, *A novel fuzzy sliding mode control approach for chaotic systems*, Iranian Journal of Fuzzy Systems, **18**(6) (2021), 133-150.

[29] K. Tahir, C. Belfedal, T. Allaoui, M. Denaï, M. Doumi, *A new sliding mode control strategy for variable-speed wind turbine power maximization*, International Transactions on Electrical Energy Systems, **28**(4) (2018), 1-22.

[30] A. T. Vo, H. J. Kang, *Adaptive neural integral full-order terminal sliding mode control for an uncertain nonlinear system*, IEEE Access, **7**(c) (2019), 42238-42246.

[31] A. T. Vo, H. J. Kang, T. D. Le, *An adaptive fuzzy terminal sliding mode control methodology for uncertain nonlinear second-order systems*, **10954** LNCS. Springer International Publishing, 2018.

[32] L. Xiong, P. Li, J. Wang, *High-order sliding mode control of DFIG under unbalanced grid voltage conditions*, International Journal of Electrical Power and Energy Systems, **117** (2020), 105608.

[33] S. S. D. Xu, C. C. Chen, Z. L. Wu, *Study of nonsingular fast terminal sliding-mode fault-tolerant control*, IEEE Transactions on Industrial Electronics, **62**(6) (2015), 3906-3913.

[34] Z. Yang et al., *Robust multi-objective optimal design of islanded hybrid system with renewable and diesel sources/stationary and mobile energy storage systems*, Renewable and Sustainable Energy Reviews, **148** (2021), 111295.

[35] Y. Yang, Y. Niu, Z. Zhang, *Dynamic event-triggered sliding mode control for interval Type-2 fuzzy systems with fading channels*, ISA Transactions, **110**(xxxx) (2021), 53-62.

[36] L. Yang, J. Yang, *Nonsingular fast terminal sliding-mode control for nonlinear dynamical systems*, International Journal of Robust and Nonlinear Control, **21**(16) (2011), 1865-1879.

[37] Y. Yu, Y. Yuan, H. Yang, H. Liu, *Nonlinear sampled-data ESO-based active disturbance rejection control for networked control systems with actuator saturation*, Nonlinear Dynamics, **95**(2) (2019), 1415-1434.